Iron ore Reduction with CO and H_2 Gas Mixtures – Thermodynamic and Kinetic Modelling

Raymond Longbottom and Leiv Kolbeinsen[1]

[1]Department of Materials Science and Engineering, Norwegian University of Science and Technology (NTNU), Trondheim, Norway

leiv.kolbeinsen@material.ntnu.no

The reduction of iron ore pellets has been studied using different techniques. Thermodynamic studies, experimental investigations and mathematical modelling have all been undertaken to better understand the behaviour of different pellet types in the new direct reduction process. The mathematical pellet model gives a good fit to most of the experimental conditions used in this work. There are some discrepancies between the experimental and calculated results under certain conditions, which are thought to be due to limitations in the experimental set up rather than fundamental issues in the model. The micromodel indicates that the hematite within the pellets is reduced to magnetite quickly, which in turn is reduced fairly quickly to wüstite. The reduction of wüstite to metallic iron seems to be the limiting stage in the reduction of the pellets, which is in line with what would be expected.

Introduction

The reduction of iron ore pellets has been studied using different techniques. Thermodynamic studies, experimental investigations and mathematical modeling have all been undertaken to better understand the behavior of different pellet types in the new direct reduction process.

Experimentally, it can be seen that the pellets reduce quickly under the proposed conditions. However, the reaction is very endothermic and causes a large temperature drop in the sample under the small scale (250 g) conditions that have been studied. The experimental equipment gives consistent results with good repeatability. A single pellet (or particle) model (the micro model) is integrated into a model for the whole process as well as for the pellets in the retort of a laboratory scale Thermo Gravimetric Analyser (TGA), and this facilitates the following main applications:

1. Combining mathematical model of retort samples of ~100 single pellet with TGA measurements allow for determination of parameters of the equations describing the resistances in the model
2. Combining mathematical model retort samples with mathematical model of process makes it possible to calculate profiles of gas concentration and temperature distributions in the process (e. g. shaft).
3. Computed gas and temperature profiles can be used to control input values to the TGA, and the resulting recorded change of sample weight as function of time and result of investigations of the pellet sample after the experiment will give extra verifications of the model and parameters
4. Effects of changing the gas & temperature profiles by alternative methods for Syn Gas (SG) and Carbon Capture (CC) as well as alternative process schemes (e. g. Wiberg) can be investigated through computer model simulations and verified experimentally using the TGA.

A robust and flexible model for reduction/oxidation is, of course together with the TGA, the core of a laboratory investigation of possible ways of integrating and verifying knowledge and competence on both the micro and the macro scales of this type of processes.

Model overview

The most frequently used reduction gases are CO and H_2.

Reduction with CO: When the initial state is hematite, and the temperature is over 570°C, reduction of iron oxide will occur in three steps:

$$\overset{\text{I}}{Fe_2O_3} \Rightarrow \overset{\text{II}}{Fe_3O_4} \Rightarrow \overset{\text{III}}{FeO} \Rightarrow Fe$$

Reactions at 25°C are:

$$3Fe_2O_3 + CO \rightleftarrows 2Fe_3O_4 + CO_2 \quad \Delta H^{\circ}_{298} = -7.8\,kJ/molFe$$

$$Fe_3O_4 + CO \rightleftarrows 3FeO + CO_2 \quad \Delta H^{\circ}_{298} = +11.2\,kJ/molFe$$

$$FeO + CO \rightleftarrows Fe + CO_2 \quad \Delta H^{\circ}_{298} = -15.7\,kJ/molFe$$

Summing these reactions gives reduction of hematite to iron:

$$Fe_2O_3 + 3CO \rightleftarrows 2Fe + 3CO_2 \quad \Delta H^{\circ}_{298} = -13.3\,kJ/molFe$$

Since wüstite is meta-stable below ~570°C, reduction should occur in only two steps below this temperature. Magnetite reduces directly to metallic iron without first being converted to wüstite:

$$Fe_3O_4 + 4CO \rightleftarrows 3Fe + CO_2 \quad \Delta H^{\circ}_{298} = -4.5\,kJ/molFe$$

Reduction with H_2: This reduction is similar to the one with CO. It occurs in three steps when temperatures are over 570°C and two steps when the temperature is below 570°C:

$$3Fe_2O_3 + H_2 \rightleftarrows 2Fe_3O_4 + H_2O_{(g)} \quad \Delta H^o_{298} = -1.0\,kJ/molFe$$

$$Fe_3O_4 + H_2 \rightleftarrows 3FeO + H_2O_{(g)} \quad \Delta H^o_{298} = +24.9\,kJ/molFe$$

$$FeO + H_2 \rightleftarrows Fe + H_2O_{(g)} \quad \Delta H^o_{298} = +25.4\,kJ/molFe$$

$$Fe_3O_4 + 4H_2 \rightleftarrows Fe + 4H_2O_{(g)} \quad \Delta H^o_{298} = +50.4\,kJ/molFe$$

$$Fe_2O_3 + 3H_2 \rightleftarrows 2Fe + 3H_2O_{(g)} \quad \Delta H^o_{298} = +49.4\,kJ/molFe$$

If one compares the Baur-Glassner diagrams in Figure 1 below it is seen that from gas utilisation point of view hydrogen is the best reduction gas dealing with high temperatures, while CO-gas is the best at low temperatures. From an enthalpy view point, hydrogen reduction is generally endothermic, and reduction with carbon monoxide is generally mildly exothermic.

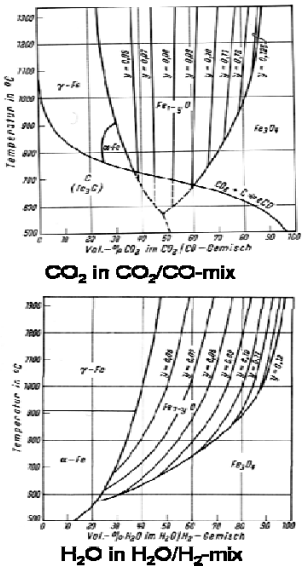

Figure 1: a) Stability of iron oxides as function of temperature and oxygen potential, b) Baur-Glassner diagrams show realisation of oxygen potential in form of CO2- and H2O-content in mixtures with CO and H2 respectively.

Reduction with CO-H_2 mixture: Often a mixture between the two gases, CO and H_2, are used as reduction gas. The ratio between C/H varies dependent on source and "production-route". The most interesting source is the use of natural-gas, methane. It is not possible to use methane as it is; it must be converted to CO and H_2. This occurs by using partial combustion or reforming with CO_2 and/or H_2O.

Partial combustion:

$$2CH_4 + O_2 = 2CO + 4H_2 \quad \Delta H^o_{298} = -35.7\,kJ/mol\,CH_4$$

Reforming:

$$CH_4 + CO_2 = 2CO + 2H_2 \quad \Delta H^o_{298} = 247.3\,kJ/mol\,CH_4$$

$$CH_4 + H_2O = CO + 3H_2 \quad \Delta H^o_{298} = 206.2\,kJ/mol\,CH_4$$

When both CO and H_2 are present all the reaction will occur so that the Water Gas Shift Reaction (WGS) equilibrium:

$$CO + H_2O = CO_2 + H_2 \quad \Delta H^o_{298} = -41.1\,kJ/mol$$

is satisfied. This reaction moves excess oxygen between the "c- and h- part" of the gas mixture, without any changes in oxidation degree of the gas.

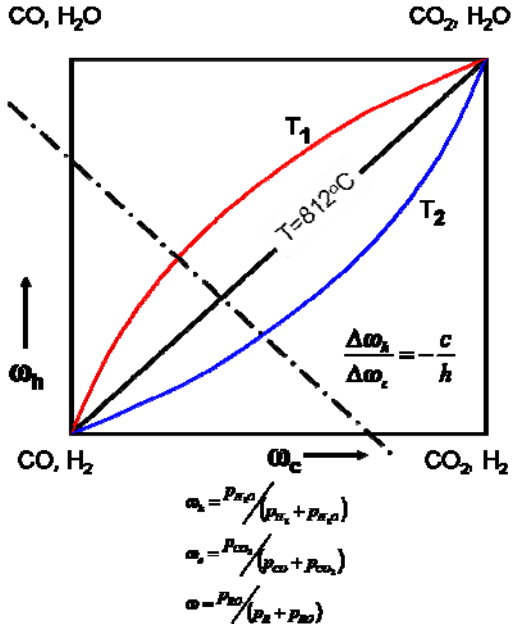

Figure 2: Water Gas Shift Reaction (WGSR) equilibrium diagram in general; definition of variables. R denotes unoxidized gas species (CO + H2) and RO denotes the oxidised gas species (CO2 + H2O). Temperature axis is normal to the paper and T2 is lower than T1.

The "dash-dot" line in Figure 2 indicates the WGSR equilibrium line for a gas mixture with given c/h-ratio and a given degree of oxidation (ω) in the gas. Using R for the unoxidized gas species (CO + H_2) and RO for the oxidised gas species (CO_2 + H_2O) this line is given by:

$$\omega_h = -\frac{c}{h}\omega_c + \omega$$

Temperature change will shift the equilibrium position along this line depending on temperature, while oxygen pick-up by the gas will move the line to the right on the diagram without changing its slope. The slope will change as a result of e.g. carburisation of solids or removal of water or carbon dioxide from the gas.

Model description

Reduction of a pellet can roughly be depicted by the well known Shrinking Core Model (SCM), but this needs to be modified to include the intermediate products magnetite and wüstite that exist between hematite and metallic iron. A single pellet is represented as a small ball with hematite in the centre followed by magnetite, wüstite and then metallic iron in concentric layers. The reducing gas in the model should at least have two active components; hydrogen and carbon monoxide, and should include the

possible internal gas reactions like the water gas shift reaction (WGSR).

The classical SCM needs to be modified both with respect to the solids, but also with respect to the gas. Earlier work at NTNU [1] - [6] has shown that the oxygen potentials in the gas and solids can replace gas compositions in this type of modelling.

It should also be noted that the mathematical model of course should be formulated as a set of time dependent differential equations in some way and it should have a clearly defined interface with the surroundings; mainly input and output gas compositions and amounts per unit volume. This is shown in Figure 3.

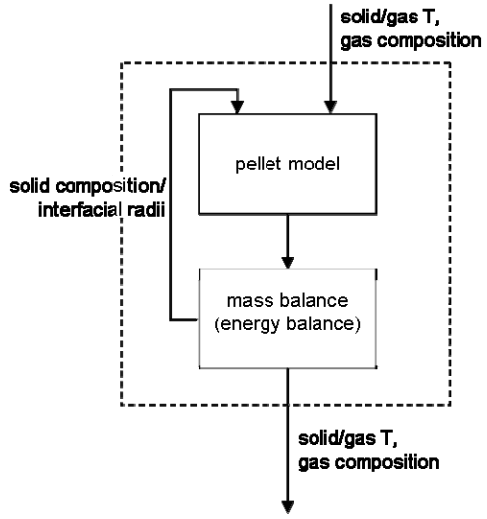

Figure 3: Flow sheet for the mathematical model of pellet reduction, showing inputs and outputs.

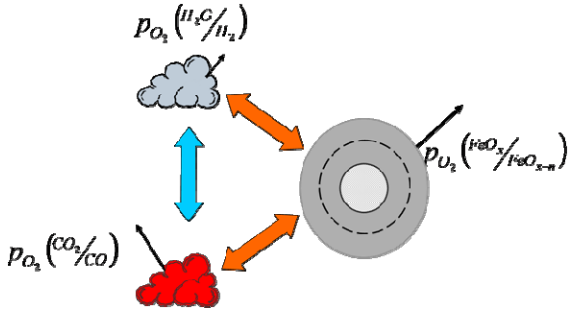

Figure 4: Clouds indicate gas mixtures and reactions internally (homogeneous or catalytic heterogeneous) transferring oxygen according to the water gas shift equation (WGSR). Oxygen transfer between gas and solid is also indicated. Numerical values for the oxygen potentials depend on compositions as well as temperatures.

Based on the above the reduction and oxidation of iron-oxygen compounds may be visualized as driven by differences in oxygen potentials set up by gas mixtures involved and the solids. This is shown in Figure 4.

The reaction:

$FeO_{x\,(s)} + R_{(g)} = FeO_{x-1\,(s)} + RO_{(g)}$ (eq.1)

can be split into two reactions, one involving the solids, and the other involving the gases:

$FeO_{x\,(s)} = FeO_{x-1\,(s)} + ½O_{2\,(g)}$ (eq.2)

$R_{(g)} + ½O_{2\,(g)} = RO_{(g)}$ (eq.3)

The Gibbs free energy of equation 1 is given by

$$\Delta G_1 = \Delta G^\circ_1 - RT \ln \frac{p_R}{p_{RO}} \quad \text{(eq.4)}$$

while for equations 2 and 3

$$\Delta G^\circ_2 = RT \ln \frac{1}{p_{O_{2(s)}}^{1/2}} \quad \text{(eq.5)}$$

$$\Delta G^\circ_3 = RT \ln \frac{p_R \cdot p_{O_{2(g)}}^{1/2}}{p_{RO}} \quad \text{(eq.6)}$$

Since equations 2 and 3 combine to give the whole reaction, the standard Gibbs free energy can be given by:

$$\Delta G^\circ_1 = RT \ln \frac{1}{p_{O_{2(s)}}^{1/2}} + RT \ln \frac{p_R \cdot p_{O_{2(g)}}^{1/2}}{p_{RO}}$$

$$= -\frac{RT}{2} \ln p_{O_{2(s)}} + \frac{RT}{2} \ln p_{O_{2(g)}} + RT \ln \frac{p_R}{p_{RO}} \quad \text{(eq.7)}$$

and substituting into equation 22, we get:

$$\Delta G_1 = \left(-\frac{RT}{2} \ln p_{O_{2(s)}} + \frac{RT}{2} \ln p_{O_{2(g)}} + RT \ln \frac{p_R}{p_{RO}} \right) - RT \ln \frac{p_R}{p_{RO}}$$

$$= \frac{RT}{2} \left(\ln p_{O_{2(g)}} - \ln p_{O_{2(s)}} \right) \quad \text{(eq.8)}$$

This difference gives the driving force for the reduction of the iron oxides by the reducing gas. It allows the computation of the driving force of reduction by both hydrogen-water vapour mixtures and carbon monoxide-carbon dioxide mixtures concurrently. A similar consideration can be used for the water gas shift reaction, giving a driving force of the difference in the $\ln p_{O_2}$ of the CO/CO_2 and H_2/H_2O fractions of the gas. This allows us to calculate reaction rates for both gases simultaneously, with the gas compositions linked through the water gas shift reaction.

In the shrinking core model, there are three processes that can govern the reaction rate: the diffusion of the reducing and product gas through the gas boundary layer surrounding the pellet; the diffusion of the gas through the product layers formed during reduction, within the pellet to the reaction interface; and the rate of the reaction itself at the interface

between the reduced and raw material. Which of these is the most important during the reduction of the pellet depend upon the temperature, the composition of the reducing gas and the physical properties of the pellet.

Since the gas atmospheres that are utilised in the model and experiments has two pairs of reducing gases, as well as inert gas, there is an adjustment in the model to reflect this. This is done by calculating the fractions of the total gas that contain $CO+CO_2$ and H_2+H_2O, and using these as multipliers for the rates of the appropriate equations.

The derived kinetic rate equations for the different processes each contain three main sections. There are:

a geometric term, which is usually the surface area of the interface at which the process is occurring;

a resistance term, which is the appropriate kinetic rate- or diffusion-coefficient, which we have incorporated as an Arrhenius expression, which allows the effect of temperature to be considered; and

a driving force, which in this case is the thermodynamic driving force, given by the difference in the logarithm of the oxygen potentials for the process.

To allow for simpler calculation of the rates of reaction, an electrical equivalent was formed of the reduction. The 'circuit' diagram for the reduction of a pellet is show in Figure 5. The individual branches of the circuit are named in the figure caption.

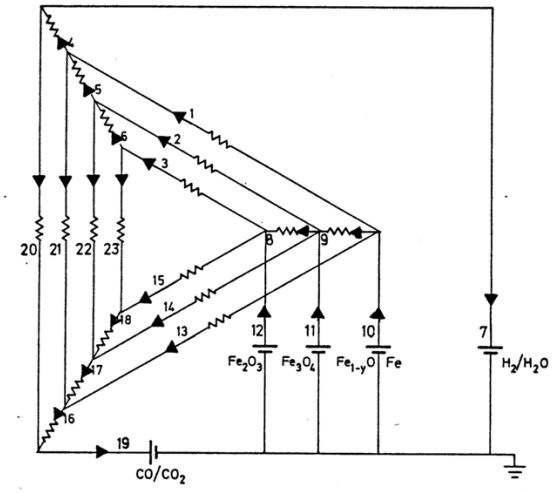

Figure 5: Electric analogue for reduction of hematite pellets. "Batteries" are representing the equilibrium oxygen potentials for gas mixtures (7, 19) and solid solutions (10, 11, and 12). Reduction with hydrogen of wüstite (1), magnetite (2), and hematite (3) will all produce water, and oxygen (as water) is transported out of the interior parts of the pellet through resistances in the product layers (4, 5, and 6). A parallel set of branches illustrates the reduction (13, 14, and 15) by carbon monoxide and oxygen transport (16, 17, and 18). Branches 21, 22, and 23 are representing WGSR on the three solid reactant/product interfaces, while branch 20 is for WGSR in the bulk gas. Four possibilities for this reaction are necessary due to varying catalytic properties of the solids compared to the bulk gas conditions. Finally, branches 8 and 9 are solid state diffusion through the magnetite and wüstite layers.

In the above consideration, hydrogen refers to the hydrogen-water vapour mixture, with the same for carbon monoxide. The geometric and resistance terms of the reaction rate equations are combined in the **G**-matrix. The driving force for the reaction is placed into the **e**-vector, while the reactions rates are given in the calculated **i**-vector. The reaction rates are given by:

$$\mathbf{i = G(u + e)} \qquad \text{(eq.9)}$$

where u describes the drop in the potential across each branch in the circuit, which is also an unknown. To eliminate u as an unknown in equation 9, another matrix Q is defined. The Q-matrix is defined using electrical circuit theory. The vector u can be given by:

$$\mathbf{u = Q^T \cdot v} \qquad \text{(eq.10)}$$

where v is voltage drop across the columns of the Q-matrix, which can be expressed in terms of the known e, G and Q. Using Kirchhoff's Law,

$$\mathbf{Q \cdot i} = 0 \qquad \text{(eq.11)}$$

and multiplying the rate equation 9 by Q and substituting in equation 10, we get:

$$\mathbf{Q \cdot i = Q \cdot G(u + e)}$$
$$0 = \mathbf{Q \cdot G(Q^T \cdot v + e)}$$
$$\mathbf{v = -(Q \cdot G \cdot Q^T)^{-1} Q \cdot G \cdot e} \qquad \text{(eq.12)}$$

Which, substituting back into equation 9, gives as the reaction rates based on the known quantities e, G and Q.

$$\mathbf{i = G(1 - Q^T(Q \cdot G \cdot Q^T)^{-1} Q \cdot G)e} \qquad \text{(eq.13)}$$

The e-vector and the G- and Q-matrices are defined in the appendix.

The general mass balance equation is

$$\frac{\partial C_j}{\partial t} + \nabla N_j = R_j^* \qquad \text{(eq.14)}$$

where the first term is the accumulation or depletion with time of species j in the pellet; the second term is the transport of j in and out of the pellet; and R_j^* is the total rate of formation or consumption of the species j in the appropriate reactions.

In the simulation of the reduction of a single pellet, there is no mass transport of solid phases in or out of the unit volume. The mass transport of the gaseous phases is already included within the micro model. In this case, we can neglect the transport term in equation 14. R_j^* is calculated by the summation of the appropriate terms in the vector i. Because i is in terms of moles, the sum of the terms of i is divided by the unit volume to give a concentration. It is also necessary to take into account the stoichiometry of the reactions. For the numerical simulation, we

discretise the differential. This gives a mass balance equation of:

$$\Delta C_j = \frac{\Delta t}{\Delta V}\left(x_{j-1}\left(\mathrm{i}_{CO}^{j-1} + \mathrm{i}_{H_2}^{j-1}\right) + x_j\left(\mathrm{i}_{CO}^{j} + \mathrm{i}_{H_2}^{j}\right)\right)$$

where x_{j-1} is the stoichiometry of the reaction of formation of the species j; x_{j-1} is the stoichiometry of the reaction of consumption of the species j; i_k^{j-1} is the element of the i-vector for the formation of j with the gas k; and similarly i_k^{j} is the element of the i-vector for the consumption of j with the gas k.

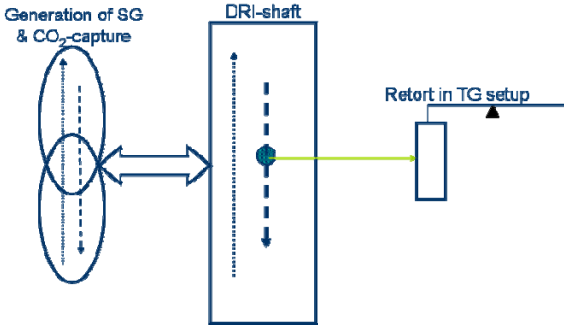

Figure 6: Interaction between two (three) counter current processes with different time constants

This single pellet (or particle) model (the micro model) is integrated into a model for the whole process as well as for the pellets in the retort of a laboratory scale Thermo Gravimetric Analyser (TGA), and this facilitates the following main applications:

1. Combining mathematical model of retort samples of ~100 single pellet with TGA measurements allow for determination of parameters of the equations describing the resistances in the model
2. Combining mathematical model retort samples with mathematical model of process makes it possible to calculate profiles of gas concentration and temperature distributions in the process (e. g. shaft).
3. Computed gas and temperature profiles can be used to control input values to the TGA, and the resulting recorded change of sample weight as function of time and result of investigations of the pellet sample after the experiment will give extra verifications of the model and parameters
4. Effects of changing the gas & temperature profiles by alternative methods for Syn Gas (SG) and Carbon Capture (CC) as well as alternative process schemes (e. g. Wiberg) can be investigated through computer model simulations and verified experimentally using the TGA.

A robust and flexible model for reduction/oxidation is, of course together with the TGA, the core of a laboratory investigation of possible ways of integrating and verifying knowledge and competence on both the micro and the macro scales of this type of processes.

Results of Reduction Experiments

Several experiments have been performed to date on the KPRS pellets supplied by LKAB and CVRD pellets supplied by Arcelor Mittal. The sample size of pellets in all experiments was a nominal 250g (~50 KPRS pellets or ~30 CVRD pellets).

Main gas mixtures used in experiments are indicated in Figure 7 and Table I below

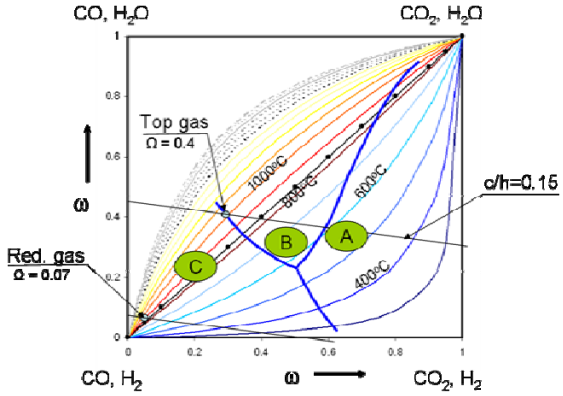

Figure 7: Gas mixtures used in experimental investigations

Table I Gas Mixtures

Gas	ω c	ω h	ω	c/h	Temperature range (°C)
"A"	0.33	0.41	0.40	0.14	435 - 500
"B"	0.50	0.30	0.33	0.14	700 - 760
"C"	0.00	0.07	0.06	0.14	880 - 910

Gas "A" is only able to reduce hematite to magnetite and will generally only apply to the upper parts of a reduction shaft. Gas "B" can also reduce the magnetite to wüstite, but will not be able to produce iron. The last gas composition, "C", is able to produce iron, but is somewhat oxidized relative to the input reduction gas as seen in Figure 7.

Generally speaking laboratory experiments were run in three different modes:

1. **Steady state conditions:** Keeping gas and temperature constant throughout the duration of the experiment. This is of course a situation a pellet never will experience on the decent through a DRI shaft, but such experiments are useful for setting initial values for adjustable model parameters.
2. **Step change conditions:** Both temperature and gas compositions are changed stepwise during the experiment but kept constant between steps. Again a situation not found in a real process, but useful for fine tuning the model parameters and investigate the robustness of the mathematical model calculations.
3. **Continuously changing conditions:** Both temperature and gas compositions are changed by ramping between the step values used under 2.

above during the experiment. This is a situation which closely resembles the change in temperature and gas composition a pellet will experience as it travels down a real shaft.

Below some examples of these three different experimental modes are presented.

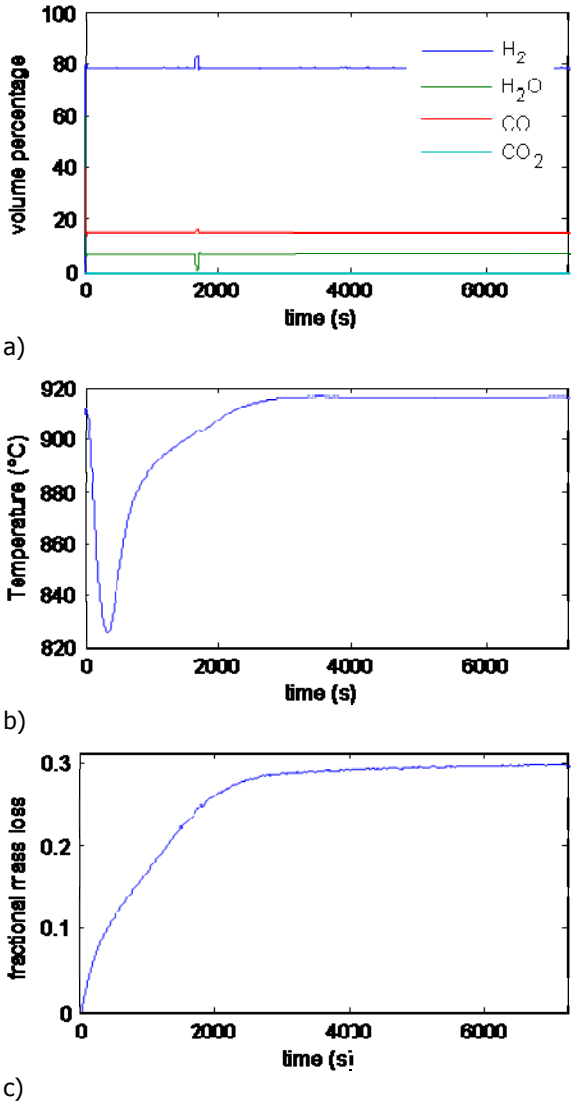

Figure 8: Results of reduction of pellets using the "constant" conditions for KPRS pellets. Experiment mode 1: a) gas composition, b) crucible temperature, c) mass change.

The temperature shown is the measured temperature, and it is noted that the crucible temperature drops significantly at the start of the experiment. This is due to the endothermic reactions when hydrogen is the dominating reducing agent. Gas composition, though, is shown to be constant. This is partly due to the fact that the gas composition shown is that of the gas mixing, but the amounts of gas supplied are at least 5 times higher than the amounts consumed by the reaction at any time.

Figure 9 shows the reduction of the pellets under the stepped change conditions, where the temperature and gas composition are stepped between the three gas compositions. The reduction rates tend to be effected much more by the change in the gas composition than the changes in temperature, which were put out of sync with each other to see the effect of each.

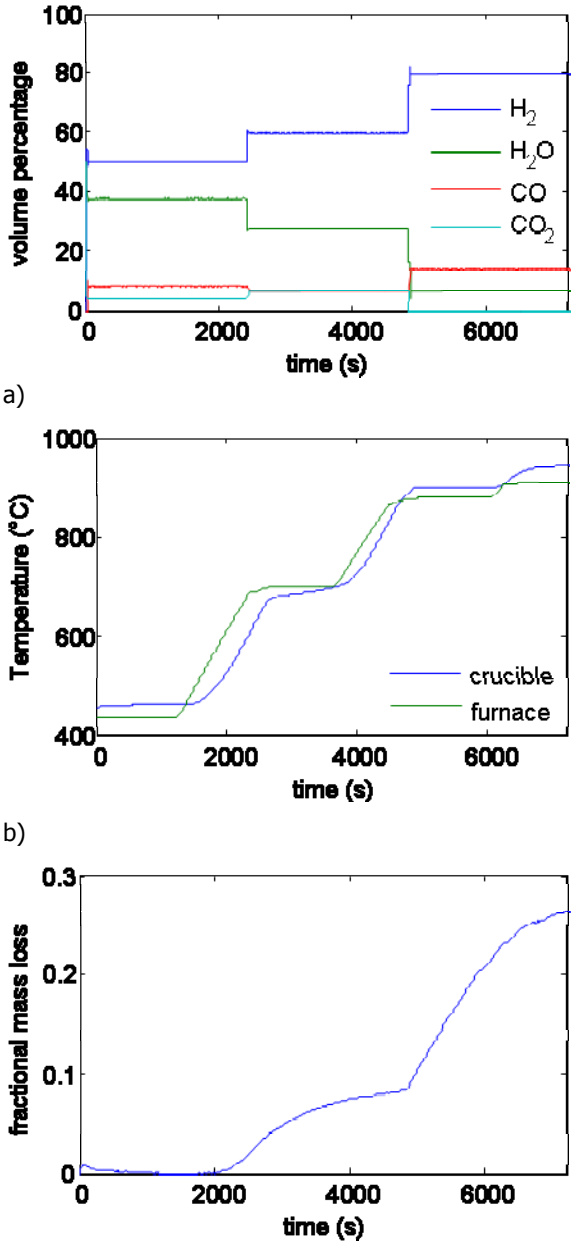

Figure 9: Results of reduction of pellets using the "step change" conditions for KPRS pellets. Experiment mode 2: a) gas composition, b) crucible temperature, c) mass change.

In this case the drop in temperature is not noticeable, partly because the rate is now determined by the change in the ability of the gas composition to reduce the various oxides, but also to the lowered rate in the experiment due to the lower temperatures used for most of time.

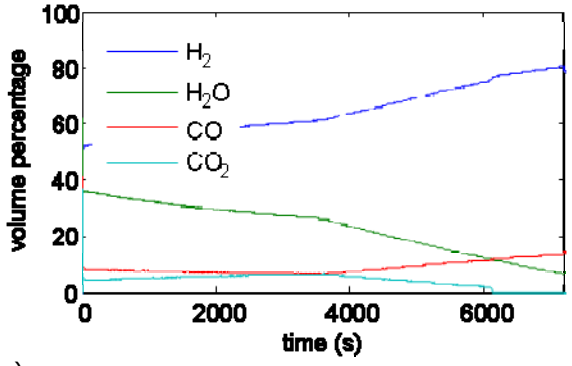

a)

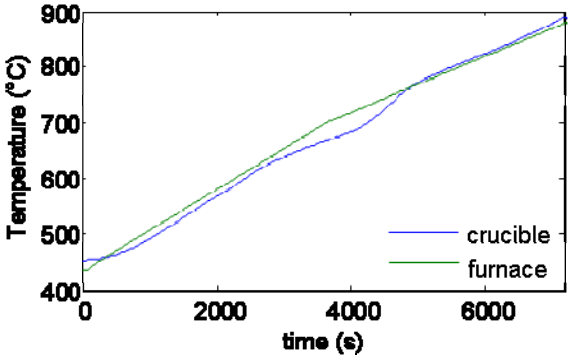

b)

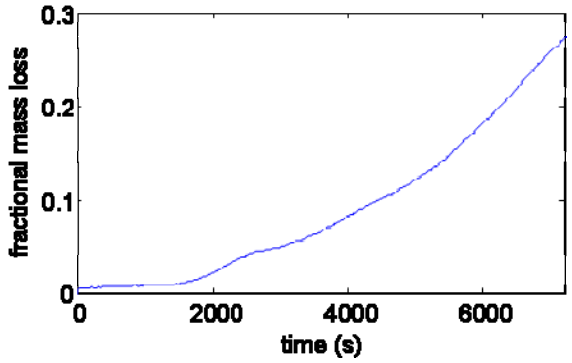

c)

Figure 10: Results of reduction of pellets using the "ramp change" conditions for KPRS pellets. Experiment mode 3: a) gas composition, b) crucible temperature, c) mass change.

Figure 10 shows the reduction of the pellets under the ramped change conditions, where the temperature and gas composition are ramped between the three conditions "A", "B", and "C". Again the changes in temperature are put out of sync with the changes in gas composition to see the effect of each.

Results of Mathematical Modelling

The modelling completed so far has been comparisons between the single pellet micro model and the experimental results indicated in the previous section. For these tests, the inputs into the model have included the gas compositions and temperature from the experimental tests at each time step. The purpose of this is to calibrate the parameters within the micro model to the experimental results, so that the micro model can be used as a part of the greater shaft model.

The parameters that can be adjusted within the model to give a better fit to the experimental results include kinetic rate constants for all of the reduction reactions as well as for the water gas shift reaction, diffusion coefficients for both gases through the product layers, and the activation energies for the reactions, although the values of these have been taken from literature and will hopefully not need to be adjusted. As such there are many degrees of freedom to adjust the model, so that fitting of the model to the experimental results should be good, but the "fundamental" nature of these parameters may give some understanding in the reduction the pellets.

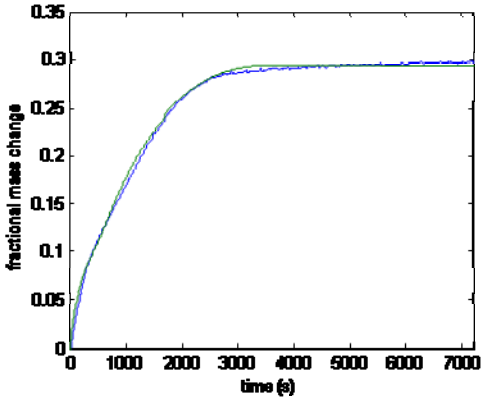

a)

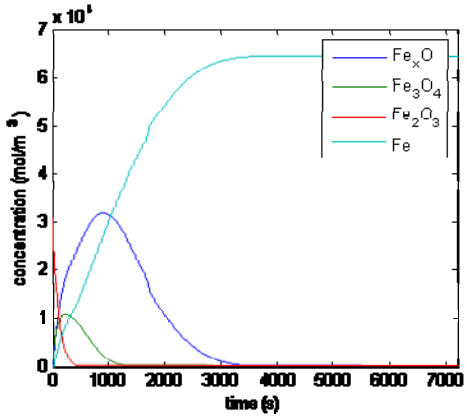

b)

Figure 11: Comparison between the experiment and the results of the micro model for the KPRS pellets reduced using the Gas "C" conditions (Mode 1). a) the experimental fractional mass loss is compared to the model; b) the calculated concentrations of the different iron species is shown. Inputs as in Figure 8

Figure 11 shows the results of the modelling of the reduction of KPRS pellets using Gas C (as shown in Figure 7) with the inputs to the model, taken from the experimental log. Under these conditions, a close fit between the model and the experimental results can be achieved fairly easily.

From the model, it can be seen that the hematite is reduced quickly, and disappears from the system early in the reduction. Wüstite and metallic iron are produced from early on during the reduction, meaning that the magnetite concentration is limited in

extent, and disappears after around 20 minutes or so. Wüstite to iron seems to be the main limiting reaction, but still occurs quickly. As the concentration of wüstite within the pellet decreases, the rate of reaction also decreases, until the reaction virtually stops after about an hour when the reaction is largely complete.

The results from modelling the reduction of KPRS pellets under the step change conditions are shown in Figure 12. Under these conditions, a reasonable match between the experimental and the calculated results can be achieved, with only a little tuning from the kinetic parameters found from the previous three experiments. The biggest deviations are at the beginning of the reduction, where the "induction" period is again noticed at low temperatures with Gas A present. However, at higher temperatures, and with increasingly reducing gases, the two curves match much better.

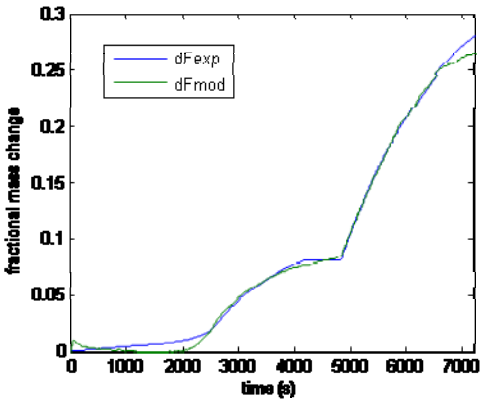

a)

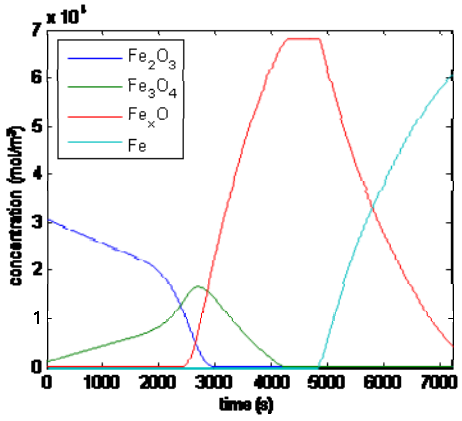

b)

Figure 12: Comparison between the experiment and the results of the micro model for the KPRS pellets reduced using the step change conditions (Mode 2). a) the experimental fractional mass loss is compared to the model; b) the calculated concentrations of the different iron species is shown. Inputs as in Figure 9

Figure 13 shows the results from the modelling of the reduction of KPRS pellets under the continuously changed (ramped) gas atmospheres and temperatures. In this case, it was much harder to find a reasonable match between the experimental and calculated fractional mass loss curves. For the current fit, the kinetic parameters were significantly increased from those in the previous simulations.

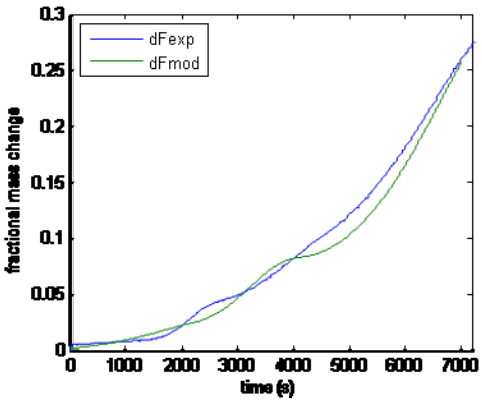

a)

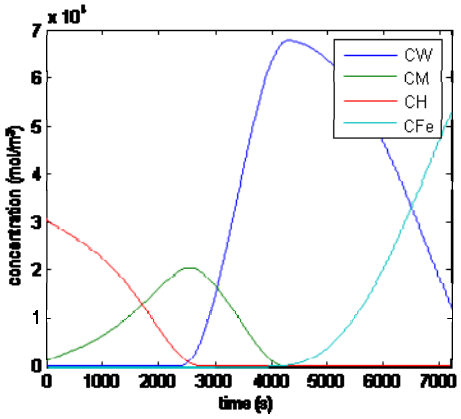

b)

Figure 13: Comparison between the experiment and the results of the micro model for the KPRS pellets reduced using the ramp change conditions (Mode 3). a) the experimental fractional mass loss is compared to the model; b) the calculated concentrations of the different iron species is shown. Inputs as in Figure 10

Even now, it can be seen that the fit and shape of the curves are somewhat different between the experimental data and what is calculated. While the three different curves that were mentioned in the previous section are simulated, their positions are different, with the flattening of the reduction curves occurring at lower extents of reduction and lower reaction times in the model than in the experiment. The positions of these cannot be easily changed without changing the thermodynamics of the model, as they are caused by a delay in the onset of the formation of wüstite and metallic iron respectively.

It is thought that in this case, the differences in the perceived thermodynamics of the model and the experiment are caused by temperature gradients within the sample, caused by the heating of the sample during the experiment. Also, the effect of slight differences between the actual and logged gas atmosphere would also be exaggerated in this case as opposed to having a constant gas atmosphere.

The effect of the temperature gradients can be reduced by repetition of the experiments, since the

vertical tube furnace used for these experiments has been replaced with an exposed element muffle furnace, which has a larger isothermal zone. The new furnace is also capable of faster heating and cooling rates, which should allow better control of the crucible temperature in the future.

Figures showing results for similar experiments and simulations for the CVRD pellets are omitted here. There is little difference between the two cases, with similar kinetic parameters used for these pellets. Since the model takes into account the different pellet diameters, the main difference noticed in the experimental results between the two pellet types does not have such a large effect on the model.

Also omitted are the results from simulations of a full shaft model. In this model the micro model plays a significant role in the mass balances for both gas and solids, as well as for the energy balances for the same [2], [7], [8] an important feature of the shaft model is the fact that it is a dynamic description where said balances are on partial differential form. In fact we may say that the micro model presented here is contained in a rudimentary macro model (shaft model) containing only one cell and described by equation 14 given earlier.

A dynamic shaft model allows starting the simulation from a known situation, e. g. a cold shaft filled with hematite pellets, and run it until a steady state is reached.

Conclusion

The reduction of iron ore pellets has been studied using different techniques. Thermodynamic studies, experimental investigations and mathematical modelling have all been undertaken to better understand the behaviour of different pellet types in the new direct reduction process developed as part of the ULCOS project [7], [8].

Experimentally, it can be seen that the pellets reduce quickly under the proposed conditions. However, the reaction is very endothermic and causes a large temperature drop in the sample under the small scale (250 g) conditions that have been studied. The experimental equipment gives consistent results with good repeatability. However, may be some problems during non-isothermal experiments, which have hopefully been rectified by the replacement of the furnace. Some further experiments will be carried out, mostly of partial reduction of the pellets, so that these pellets can be characterised and used as a further comparison and check for the mathematical model.

The mathematical pellet model is working, and can give a good fit to most of the experimental conditions used in this work. There are however, some discrepancies between the experimental and calculated results under certain conditions, which are thought to be due to limitations in the experimental set up rather than fundamental issues in the model. The micro model indicates that the hematite within the pellets is reduced to magnetite quickly, which in turn is reduced fairly quickly to wüstite. The reduction of wüstite to metallic iron seems to be the limiting stage in the reduction of the pellets, which is in line with what would be expected.

The shaft model is working, but with known issues. Some further work is required for this model to work satisfactorily, but this is not envisioned to be an extensive task for a simple shaft model. It should be noted, however, that the formulation chosen for the micro model described, as well as its interaction with the surroundings is done in a manner intended to facilitate any chosen complexity in the shaft model.

Acknowledgements

Grant number 158907 from the Norwegian Research Council for the project "DISvaDRI - Dispersoids In Steel and value added Direct Reduced Iron" in the SIPNMATR program for allowing use of TGA equipment. Research scientist, Dr. Sean Gaal is thanked for his efforts in continuously improving the performance of said TGA equipment.

References

[1] Kolbeinsen, L.: "Reduction of Iron Ore – Mathematical model for process control". PhD - thesis, Metallurgisk Institutt NTH May 1982 (In Norwegian)

[2] Kolbeinsen, L. & Onshus, T.: "Reduction of Iron Pellets in a Shaft furnace - A Dynamic Approach". Proc. of the 6th Process Technology Conf. - Fifth International Iron and Steel Congress, pp. 37-43, Washington April 1986.

[3] Kolbeinsen, L. & Onshus, T.: "A generalized Shrinking Core Model including the Water Gas Shift Reaction applied to Reduction of Hematite Pellets". Proc. of The fourth Japan-Nordic Countries joint Symposium on Science and Technology of Process Metallurgy, The Iron and Steel Institute of Japan, pp. 66-80, Tokyo, November 1986.

[4] Leiv Kolbeinsen: "Metallurgical Conversion of Natural Gas" Proc. of The Fifth Japan-Nordic Countries joint Symposium on Science and Technology of Process Metallurgy, Sept. 1992, Helsinki, Finland, pp 191-207

[5] Kolbeinsen, L. & Båsen, T.: "FERROCARBON - Production and use of Iron Carbide" Proc. of the 2. Int. Symp. on Metallurgical Processes for the Year 2000 and Beyond and the 1994 TMS Extraction and Process Metallurgy Meeting . San Diego, September 1994

[6] Tveit, H. & Kolbeinsen, L.: "Export Processed Gas!" (In Norwegian) Teknisk Ukeblad Teknikk 142 (11) March 1995 pp 28-29

[7] Leiv Kolbeinsen: "Summary of SP3 activities at Department of Materials Science and Engineering, NTNU" ULCOS//SP3 RTD/WP3.2&3.3/ntnu 2006c

[8] Leiv Kolbeinsen & Ray Longbottom: "Summary of SP12 activities at Department of Materials Science and Engineering, NTNU" ULCOS//SP12 RTD/ ntnu 2008

Appendix – Definition of Vectors and Matrices used in the Micromodel

Nomenclature

C_i	molar concentration of compound *i*
C_c	molar concentration of the carbon containing fraction of the gas (CO + CO_2)
C_h	molar concentration of the hydrogen containing fraction of the gas (H_2 + H_2O)
$D^J_{eff,i}$	effective binary diffusion of gas fraction *i* through solid *J*
$E^J_{a,i}$	activation energy for reduction to *J* by gas *i*
E^{WGS}_a	activation energy for the water gas shift reaction
k_f	mass transfer coefficient through the gas boundary layer
$k^J_{o,i}$	frequency factor in Arrhenius equation for reduction to *J* by gas *i*
k^J_o	frequency factor in Arrhenius equation for the water gas shift reaction at the inner interface of solid *J* or bulk gas
N_j	moles of species *j*
R	gas constant
R^*_j	total rate of formation/consumption of species *j* in the relevant reactions
r_J	radius of reaction interface at the inner surface of solid *J*
r_o	radius of pellet
T	Temperature
t	Time
ΔG°_J	Gibbs free energy of reduction to *J* in the solid phase
ΔG°_i	Gibbs free energy of the fraction in the gas phase containing *i*

Superscripts

g	bulk gas phase
Fe	metallic iron
M	Magnetite
W	wüstite

Subscripts

c	carbon containing fraction of gas
h	hydrogen containing fraction of gas
Fe	metallic iron
M	Magnetite
W	wüstite

Table A-1: Diagonal terms of the **G**-matrix (dimension 23×23), all others are zero.

Term	Equation	Remark
G(1,1)	$C_h k_{o,h}^{Fe} \exp\left(\frac{-E_{a,h}^{Fe}}{RT}\right) 2\pi {r_W}^2 RT$	interfacial reduction of Fe_xO with H_2
G(2,2)	$C_h k_{o,h}^{W} \exp\left(\frac{-E_{a,h}^{W}}{RT}\right) 2\pi {r_M}^2 RT$	interfacial reduction of Fe_3O_4 with H_2
G(3,3)	$C_h k_{o,h}^{M} \exp\left(\frac{-E_{a,h}^{M}}{RT}\right) 2\pi {r_H}^2 RT$	interfacial reduction of Fe_2O_3 with H_2
G(4,4)	$\frac{1}{\left(\frac{r_o - r_{Fe}}{D_{eff,h}^{Fe} \cdot 2\pi r_{Fe} r_o RT}\right) + \left(\frac{1}{k_f^h \cdot 2\pi {r_o}^2 RT}\right)}$	diffusion of H_2/H_2O through boundary layer & Fe-layer
G(5,5)	$D_{eff,h}^{W} \cdot 2\pi r_W r_{Fe} RT \left(\frac{1}{r_{Fe} - r_W}\right)$	diffusion of H_2/H_2O through Fe_xO-layer
G(6,6)	$D_{eff,h}^{M} \cdot 2\pi r_M r_W RT \left(\frac{1}{r_W - r_M}\right)$	diffusion of H_2/H_2O through Fe_3O_4-layer
G(7,7)	∞	potential of H_2/H_2O in gas phase
G(8,8)	0	solids diffusion in Fe_3O_4
G(9,9)	0	solids diffusion in Fe_xO
G(10,10)	∞	potential of solids at Fe_xO/Fe interface
G(11,11)	∞	potential of solids at Fe_3O_4/Fe_xO interface
G(12,12)	∞	potential of solids at Fe_2O_3/Fe_3O_4 interface
G(13,13)	$C_c k_{o,c}^{Fe} \exp\left(\frac{-E_{a,c}^{Fe}}{RT}\right) 2\pi {r_W}^2 RT$	interfacial reduction of Fe_xO with CO
G(14,14)	$C_c k_{o,c}^{W} \exp\left(\frac{-E_{a,c}^{W}}{RT}\right) 2\pi {r_M}^2 RT$	interfacial reduction of Fe_3O_4 with CO
G(15,15)	$C_c k_{o,c}^{M} \exp\left(\frac{-E_{a,c}^{M}}{RT}\right) 2\pi {r_H}^2 RT$	interfacial reduction of Fe_2O_3 with CO
G(16,16)	$\frac{1}{\left(\frac{r_o - r_{Fe}}{D_{eff,c}^{Fe} \cdot 2\pi r_{Fe} r_o RT}\right) + \left(\frac{1}{k_f^c \cdot 2\pi {r_o}^2 RT}\right)}$	diffusion of CO/CO_2 through boundary layer & Fe-layer
G(17,17)	$D_{eff,c}^{W} \cdot 2\pi r_W r_{Fe} RT \left(\frac{1}{r_{Fe} - r_W}\right)$	diffusion of CO/CO_2 through Fe_xO-layer
G(18,18)	$D_{eff,c}^{M} \cdot 2\pi r_M r_W RT \left(\frac{1}{r_W - r_M}\right)$	diffusion of CO/CO_2 through Fe_3O_4-layer
G(19,19)	∞	potential of CO/CO_2 in gas phase

Table A-1 (cont.)

Term	Equation	Remark
G(20,20)	$k_o^g \exp\left(\frac{-E_a^{WGS}}{RT}\right) \cdot 2\pi r_o^{\,2} RT$	WGS reaction in gas phase
G(21,21)	$k_o^{Fe} \exp\left(\frac{-E_a^{WGS}}{RT}\right) \cdot 2\pi r_{Fe}^{\,2} RT$	WGS reaction on pellet surface & Fe_xO/Fe interface
G(22,22)	$k_o^W \exp\left(\frac{-E_a^{WGS}}{RT}\right) \cdot 2\pi r_W^{\,2} RT$	WGS reaction on Fe_3O_4/Fe_xO interface
G(23,23)	$k_o^M \exp\left(\frac{-E_a^{WGS}}{RT}\right) \cdot 2\pi r_M^{\,2} RT$	WGS reaction on Fe_2O_3/Fe_3O_4 interface

Table A-2: Terms of the **e**-vector (dimension 23), all other terms are zero.

Term	Equation	Remark
e(10)	$2\left(\frac{\Delta G_{Fe}^{\circ}}{RT}\right)$	potential of solids at Fe_xO/Fe interface
e(11)	$2\left(\frac{\Delta G_{W}^{\circ}}{RT}\right)$	potential of solids at Fe_3O_4/Fe_xO interface
e(12)	$2\left(\frac{\Delta G_{M}^{\circ}}{RT}\right)$	potential of solids at Fe_2O_3/Fe_3O_4 interface
e(7)	$-2\left(\frac{\Delta G_{H_2/H_2O}^{\circ}}{RT}\right)$	Potential of H_2/H_2O in gas phase
e(19)	$-2\left(\frac{\Delta G_{CO/CO_2}^{\circ}}{RT}\right)$	Potential of CO/CO_2 in gas phase

The **Q**-matrix (dimension 11×23) is:

Q =

$$
\mathbf{Q} = \begin{bmatrix}
1 & 1 & 1 & 0 & 0 & 0 & -1 & 0 & 0 & 0 & 0 & 0 & 0 & 0 & 0 & 0 & 0 & 0 & 0 & -1 & -1 & -1 & -1 \\
0 & 0 & 0 & 1 & 0 & 0 & -1 & 0 & 0 & 0 & 0 & 0 & 0 & 0 & 0 & 0 & 0 & 0 & 0 & -1 & 0 & 0 & 0 \\
0 & -1 & -1 & 0 & 1 & 0 & 0 & 0 & 0 & 0 & 0 & 0 & 0 & 0 & 0 & 0 & 0 & 0 & 0 & 0 & 0 & 1 & 1 \\
0 & 0 & -1 & 0 & 0 & 1 & 0 & 0 & 0 & 0 & 0 & 0 & 0 & 0 & 0 & 0 & 0 & 0 & 0 & 0 & 0 & 0 & 1 \\
0 & 0 & -1 & 0 & 0 & 0 & 0 & 1 & 0 & 0 & 0 & 1 & 0 & 0 & -1 & 0 & 0 & 0 & 0 & 0 & 0 & 0 & 0 \\
0 & -1 & -1 & 0 & 0 & 0 & 0 & 0 & 1 & 0 & 1 & 1 & 0 & -1 & -1 & 0 & 0 & 0 & 0 & 0 & 0 & 0 & 0 \\
0 & 0 & 0 & 0 & 0 & 0 & -1 & 0 & 0 & 1 & 1 & 1 & 0 & 0 & 0 & 0 & 0 & 0 & -1 & 0 & 0 & 0 & 0 \\
0 & 0 & 0 & 0 & 0 & 0 & 0 & 0 & 0 & 0 & 0 & 0 & 1 & 1 & 1 & 0 & 0 & 0 & -1 & 1 & 1 & 1 & 1 \\
0 & 0 & 0 & 0 & 0 & 0 & 0 & 0 & 0 & 0 & 0 & 0 & 0 & 0 & 0 & 1 & 0 & 0 & -1 & 1 & 0 & 0 & 0 \\
0 & 0 & 0 & 0 & 0 & 0 & 0 & 0 & 0 & 0 & 0 & 0 & 0 & -1 & -1 & 0 & 1 & 0 & 0 & 0 & 0 & -1 & -1 \\
0 & 0 & 0 & 0 & 0 & 0 & 0 & 0 & 0 & 0 & 0 & 0 & 0 & 0 & -1 & 0 & 0 & 1 & 0 & 0 & 0 & 0 & -1
\end{bmatrix}
$$